

Reentrant phase transitions of a coupled spin-electron model on doubly decorated planar lattices with two or three consecutive critical points

Hana Čenčariková^{a,*}, Jozef Strečka^b, Marcelo L. Lyra^c

^a*Institute of Experimental Physics, Slovak Academy of Sciences, Watsonova 47, 040 01 Košice, Slovakia*

^b*Department of Theoretical Physics and Astrophysics, Faculty of Science, P. J. Šafárik University, Park Angelinum 9, 040 01 Košice, Slovakia*

^c*Instituto de Física, Universidade Federal de Alagoas, 57072-970 Maceió, AL, Brazil*

Abstract

The generalized decoration-iteration transformation is adapted for the exact study of a coupled spin-electron model on 2D lattices in which localized Ising spins reside on nodal lattice sites and mobile electrons are delocalized over pairs of decorating sites. The model takes into account a hopping term for mobile electrons, the Ising coupling between mobile electrons and localized spins as well as the Ising coupling between localized spins (J'). The ground state, spontaneous magnetization and specific heat are examined for both ferromagnetic ($J' > 0$) as well as antiferromagnetic ($J' < 0$) interaction between the localized spins. Several kinds of reentrant transitions between the paramagnetic (P), antiferromagnetic (AF) and ferromagnetic (F) phases have been found either with a single critical point, or with two consecutive critical points ($P - AF/F - P$) and three successive critical points $AF/F - P - F/AF - P$. Striking thermal variations of the spontaneous magnetization depict a strong reduction due to the interplay between annealed disorder and quantum fluctuations in addition to the aforementioned reentrance. It is shown that the specific heat displays diverse thermal dependencies including finite cusps at the critical temperatures.

Keywords: strongly correlated systems, Ising spins, mobile electrons, phase transitions, criticality

1. Introduction

During the past decades the more interesting and unconventional phenomena like the giant magnetoresistivity [1–4], metal-insulator transitions [5], itinerant ferromagnetism [6–8], metamagnetic transitions [9–11], mixed-valence phenomena [5], enhanced magnetocaloric effect [12–15], superconductivity [16–18], electronic ferroelectricity [19, 20], or multiferroicity [21, 22] have attracted much attention of experimental as well as theoretical physicists with the aim to describe and explain the origin of these intriguing phenomena. In spite of enormous efforts, some of these phenomena still lack full understanding and have not been reliably explained so far. Most of the aforementioned collective phenomena arise from the mutual interaction between mobile and localized electrons, which is of a highly cooperative nature with many active degrees of freedom. In general, it is a very complex task to solve this kind of interacting many-body problem, which requires application of various alternative approaches. One of them, currently in foreground, is the application of an appropriate type of a numerical method, which can be either the exact (e.g., the exact diagonalization [23, 24]) or approximate (e.g., the Density Matrix Renormalization Group [25–27] or Monte Carlo methods [28, 29]). Another approach, which enables to investigate the physical properties of mutually coupled electron and spin subsystems, is based on first-principle calculations known as

a Density Functional Theory [30]. Although both aforementioned approaches are very useful, there are serious limitations when applying them to coupled spin-electron systems owing to restrictions related to CPU time, machine memory or other computational difficulties associated with finite-size effects.

Recently, another fascinating approach has been suggested by Pereira *et al.* [31, 32] when applying a relatively simple analytical method based on the generalized decoration-iteration transformation to an interacting spin-electron system on a diamond chain. Following Fisher's ideas [33], an arbitrary statistical-mechanical system (even of quantum nature), which merely interacts with either two or three outer Ising spins, may be replaced with the effective interactions between the outer Ising spins through the generalized decoration-iteration or star-triangle mapping transformations [33, 34]. The procedure elaborated by Pereira *et al.* [31, 32] has been later adopted to other interacting spin-electron models in one [35–42] or two dimensions [43–46]. The interest in this field of study has two different reasons. The first, very prosaic, reason is that such relatively simple procedure allows us to obtain ground states as well as thermodynamic characteristics for an interesting class of two-component spin-electron systems. These systems has gained a new direction with the realization of optical lattices [47], namely, they represent a theoretical counterpart of possible experimental realizations of coupled spin-electron systems on decorated lattices that allow us to study many types of collective phenomena in their pure nature [48–50]. The second, more crucial, reason relates to the possibility to provide important hints on fundamental questions concerning the origin of phe-

*Corresponding author:

Email address: hcencar@saske.sk (Hana Čenčariková)

nomena such as the giant magnetocaloric effect, metamagnetic transitions, reentrant phase transitions, etc.

The organization of this paper is as follows. In Sec. 2, we will first introduce a coupled spin-electron model on 2D lattices in which localized Ising spins reside on nodal lattice sites and mobile electrons are delocalized over pairs of decorating sites, together with the crucial steps of an exact mapping procedure, which has been used to obtain exact closed-form expressions for the critical temperature, order parameter and other relevant thermodynamic characteristics. The most interesting results for the ground state and the finite-temperature phase diagrams are collected in Sec. 3 along with thermal dependencies of magnetization and specific heat. In this section, our attention will be also focused on the possibility of observing reentrant phase transitions. Finally, some concluding remarks are drawn in Sec. 4.

2. Model and Method

Let us investigate an interacting spin-electron system on doubly decorated 2D lattices, as displayed in Fig. 1. The investigated model contains one localized Ising spin at each nodal lattice site and a set of mobile electrons delocalized over the pairs of decorating sites (dimers) placed at each bond (see Fig. 1). From the experimental point of view, such coupled spin-electron models could capture physical properties of polymeric coordination compounds like $[\text{Ru}_2(\text{OOCtBu})_4]_3[\text{M}(\text{CN})_6]$ ($\text{M}=\text{Fe}, \text{Cr}$) [51].

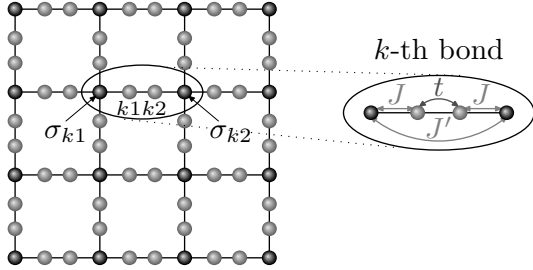


Figure 1: A schematic representation of the studied spin-electron model on a doubly decorated square lattice. Black balls represent the nodal sites occupied by the localized Ising spins and gray balls represent the decorating sites occupied by at most four mobile electrons per dimer. The ellipse illustrates the k -th bond.

In the present model, each decorating site involves a s -type orbital, which can be occupied by at most two electrons with opposite spins in accordance with the Pauli's exclusion principle. The electron motion described by the hopping amplitude t is allowed just between nearest-neighbour decorating sites. Each localized Ising spin interacts with the nearest-neighbour mobile electrons through the Ising coupling J . In the present work we go beyond the previous studies [46, 63] by taking into account the additional Ising coupling J' between nearest-neighbour localized Ising spins. We suppose that this interaction is not negligible and it can lead to a new physics in the coupled spin-electron systems due to a competition with the effective cou-

pling originating from the hopping process of the mobile electrons. The total Hamiltonian of the interacting spin-electron system on such doubly decorated 2D lattice can be written as follows

$$\hat{\mathcal{H}} = -t \sum_{k=1}^{Nq/2} \sum_{\gamma=\uparrow,\downarrow} (\hat{c}_{k1,\gamma}^\dagger \hat{c}_{k2,\gamma} + h.c.) - J \sum_{\langle ik \rangle} \hat{\sigma}_i^z (\hat{n}_{k\alpha,\uparrow} - \hat{n}_{k\alpha,\downarrow}) - J' \sum_{\langle kl \rangle} \hat{\sigma}_k^z \hat{\sigma}_l^z, \quad (1)$$

where $\hat{c}_{k\alpha,\gamma}^\dagger$ and $\hat{c}_{k\alpha,\gamma}$ ($\alpha=1,2$) are the creation and annihilation fermionic operators for the mobile electrons delocalized over the k -th decorating dimer, $\hat{n}_{k\alpha,\gamma} = \hat{c}_{k\alpha,\gamma}^\dagger \hat{c}_{k\alpha,\gamma}$ and $\hat{n}_{k\alpha} = \hat{n}_{k\alpha,\uparrow} + \hat{n}_{k\alpha,\downarrow}$ are the respective number operators. The operator $\hat{\sigma}_i^z$ denotes the z -component of the spin-1/2 operator with eigenvalues $\sigma_i^z = \pm 1$. The first term in Eq. (1) describes the quantum-mechanical hopping of mobile electrons delocalized over a couple of decorating sites $k1$ and $k2$ from the k -th dimer. The second term represents the Ising-type exchange interaction between the mobile electrons and their nearest Ising neighbours. The last term in Eq. (1) represents a further-neighbour Ising-type exchange interaction between the nearest-neighbour localized Ising spins. The symbol N denotes the total number of localized Ising spins and q is their coordination number. For a practical reason, we may rewrite the total Hamiltonian (1) in the form of a sum over bond Hamiltonians $\hat{\mathcal{H}} = \sum_{k=1}^{Nq/2} \hat{\mathcal{H}}_k$, where each bond Hamiltonian $\hat{\mathcal{H}}_k$ accounts for the kinetic energy of mobile electrons from the k -th decorating dimer, the exchange interaction between the mobile electrons and their nearest-neighbour Ising spins, and finally, the exchange interaction between two localized Ising spins attached to the k -th decorating dimer

$$\hat{\mathcal{H}}_k = -t (\hat{c}_{k1,\uparrow}^\dagger \hat{c}_{k2,\uparrow} + \hat{c}_{k1,\downarrow}^\dagger \hat{c}_{k2,\downarrow} + \hat{c}_{k2,\uparrow}^\dagger \hat{c}_{k1,\uparrow} + \hat{c}_{k2,\downarrow}^\dagger \hat{c}_{k1,\downarrow}) - J \hat{\sigma}_{k1}^z (\hat{n}_{k1,\uparrow} - \hat{n}_{k1,\downarrow}) - J \hat{\sigma}_{k2}^z (\hat{n}_{k2,\uparrow} - \hat{n}_{k2,\downarrow}) - J' \hat{\sigma}_{k1}^z \hat{\sigma}_{k2}^z. \quad (2)$$

Let us calculate the grand-canonical partition function Ξ of the correlated spin-electron system, which will allow us to rigorously analyze the ground-state as well as the thermodynamic properties. In general, the calculation of the grand-canonical partition function is a difficult problem, but for the model defined by Eq. (1) there exists an elegant way due to the commutativity between different bond Hamiltonians $[\hat{\mathcal{H}}_i, \hat{\mathcal{H}}_j]=0$. This fact allows us to partially factorize the grand-canonical partition function into the product of bond partition functions Ξ_k

$$\Xi = \sum_{\{\sigma_i\}} \prod_{k=1}^{Nq/2} \text{Tr}_k \exp(-\beta \hat{\mathcal{H}}_k) \exp(\beta \mu \hat{n}_k) = \sum_{\{\sigma_i\}} \prod_{k=1}^{Nq/2} \Xi_k, \quad (3)$$

where $\beta = 1/(k_B T)$, k_B is the Boltzmann's constant, T is the absolute temperature, $\hat{n}_k = \hat{n}_{k1} + \hat{n}_{k2}$ is the total number operator for mobile electrons delocalized over the k -th decorating dimer and μ is their chemical potential. The summation $\sum_{\{\sigma_i\}}$ in Eq. (3) runs over all possible configurations of the nodal Ising spins and the symbol Tr_k stands for the trace over the degrees of freedom of the mobile electrons from the k -th decorating dimer.

It is evident from this notation that it is necessary to diagonalize the bond Hamiltonian $\hat{\mathcal{H}}_k$ in order to find the grand-canonical partition function. Apparently, the bond Hamiltonian $\hat{\mathcal{H}}_k$ commutes with the total number of mobile electrons per bond (\hat{n}_k) as well as the z-component of the total spin of the mobile electrons $\hat{S}_k^z = \sum_{\alpha=\{1,2\}}(\hat{n}_{k\alpha,\uparrow} - \hat{n}_{k\alpha,\downarrow})$. Hence, it follows that the matrix form of the bond Hamiltonian $\hat{\mathcal{H}}_k$ can be divided into several disjoint blocks $\mathcal{H}_k(n_k, S_k^z)$ corresponding to orthogonal Hilbert subspaces characterized by different numbers of mobile electrons (n_k) and different values of the total spin S_k^z . Since the further-neighbour exchange coupling J' between the localized Ising spins (the last term in Eq. (2)) is independent of the mobile electrons, it is sufficient to diagonalize the reduced form of the bond Hamiltonian $\tilde{\mathcal{H}}_k$ including only the first two terms depending on the mobile electrons, whereas the obtained eigenvalues (\tilde{E}_k) must be subsequently extended by an additional term $-J'\sigma_{k1}\sigma_{k2}$ in order to obtain the eigenvalues E_k of the full bond Hamiltonian \mathcal{H}_k .

(a) The subspace with $n_k = 0$.

This subspace includes only one basis state, and namely, $|0, 0\rangle_k$ (the notation $|0, 0\rangle_k$ denotes the vacuum state of the pair of decorating sites on the k -th bond) with $S_k^z = 0$. Thus, the corresponding block Hamiltonian has the form $\tilde{\mathcal{H}}_k(0, 0) = 0$, which gives the eigenvalue

$$E_{k1} = -J'\sigma_{k1}\sigma_{k2}. \quad (4)$$

(b) The subspace with $n_k = 1$.

In this case, four basis states $\hat{c}_{k1,\uparrow}^\dagger|0, 0\rangle_k$, $\hat{c}_{k2,\uparrow}^\dagger|0, 0\rangle_k$, $\hat{c}_{k1,\downarrow}^\dagger|0, 0\rangle_k$, $\hat{c}_{k2,\downarrow}^\dagger|0, 0\rangle_k$ lead to two different 2×2 block Hamiltonians with the total spin $S_k^z = \pm 1$

$$\tilde{\mathcal{H}}_k(1, \pm 1) = \begin{pmatrix} \mp J\sigma_{k1} & -t \\ -t & \mp J\sigma_{k2} \end{pmatrix}, \quad (5)$$

which give, after the direct diagonalization, the following eigenvalues for $S_k^z = 1$

$$E_{k2,k3} = -\frac{J(\sigma_{k1} + \sigma_{k2})}{2} \pm \frac{\sqrt{J^2(\sigma_{k1} - \sigma_{k2})^2 + 4t^2}}{2} - J'\sigma_{k1}\sigma_{k2}, \quad (6)$$

and for $S_k^z = -1$

$$E_{k4,k5} = \frac{J(\sigma_{k1} + \sigma_{k2})}{2} \pm \frac{\sqrt{J^2(\sigma_{k1} - \sigma_{k2})^2 + 4t^2}}{2} - J'\sigma_{k1}\sigma_{k2}. \quad (7)$$

(c) The subspace with $n_k = 2$.

In this Hilbert subspace, three different block Hamiltonians can be discerned according to the value of the total spin S_k^z available to the basis states $\hat{c}_{k1,\gamma}^\dagger\hat{c}_{k2,\gamma}^\dagger|0, 0\rangle_k$. For two mobile electrons with equally oriented spins $S_k^z = \pm 2$ the bond Hamiltonians $\tilde{\mathcal{H}}_k$ take the following form

$$\tilde{\mathcal{H}}_k(2, \pm 2) = \mp J(\sigma_{k1} + \sigma_{k2}), \quad (8)$$

which directly give other two eigenvalues

$$E_{k6,k7} = \mp J(\sigma_{k1} + \sigma_{k2}) - J'\sigma_{k1}\sigma_{k2}. \quad (9)$$

The Hilbert subspace spanned over the four basis states $\hat{c}_{k1,\uparrow}^\dagger\hat{c}_{k2,\downarrow}^\dagger|0, 0\rangle_k$, $\hat{c}_{k1,\downarrow}^\dagger\hat{c}_{k2,\uparrow}^\dagger|0, 0\rangle_k$, $\hat{c}_{k1,\uparrow}^\dagger\hat{c}_{k1,\downarrow}^\dagger|0, 0\rangle_k$, $\hat{c}_{k2,\uparrow}^\dagger\hat{c}_{k2,\downarrow}^\dagger|0, 0\rangle_k$, with the opposite orientation of two mobile electrons leads to the following block Hamiltonian $\tilde{\mathcal{H}}_k$ for the particular case with $S_k^z = 0$

$$\tilde{\mathcal{H}}_k(2, 0) = \begin{pmatrix} -J(\sigma_{k1} - \sigma_{k2}) & 0 & -t & -t \\ 0 & J(\sigma_{k1} - \sigma_{k2}) & t & t \\ -t & t & 0 & 0 \\ -t & t & 0 & 0 \end{pmatrix}, \quad (10)$$

which gives the following four eigenvalues

$$E_{k8,k9} = -J'\sigma_{k1}\sigma_{k2}. \quad (11)$$

$$E_{k10,k11} = \pm \sqrt{J^2(\sigma_{k1} - \sigma_{k2})^2 + 4t^2} - J'\sigma_{k1}\sigma_{k2}. \quad (12)$$

(d) The subspace with $n_k = 3$.

There are four different basis states $\hat{c}_{k1,\uparrow}^\dagger\hat{c}_{k1,\downarrow}^\dagger\hat{c}_{k2,\uparrow}^\dagger|0, 0\rangle_k$, $\hat{c}_{k1,\uparrow}^\dagger\hat{c}_{k1,\downarrow}^\dagger\hat{c}_{k2,\downarrow}^\dagger|0, 0\rangle_k$, $\hat{c}_{k1,\uparrow}^\dagger\hat{c}_{k2,\uparrow}^\dagger\hat{c}_{k2,\downarrow}^\dagger|0, 0\rangle_k$ and $\hat{c}_{k1,\downarrow}^\dagger\hat{c}_{k2,\uparrow}^\dagger\hat{c}_{k2,\downarrow}^\dagger|0, 0\rangle_k$, which form two different 2×2 block Hamiltonians

$$\tilde{\mathcal{H}}_k(3, \pm 1) = \begin{pmatrix} \mp J\sigma_{k2} & t \\ t & \mp J\sigma_{k1} \end{pmatrix}. \quad (13)$$

After the direct diagonalization of (13) for $S_k^z = 1$, one obtains the eigenvalues

$$E_{k12,k13} = -\frac{J(\sigma_{k1} + \sigma_{k2})}{2} \pm \frac{\sqrt{J^2(\sigma_{k1} - \sigma_{k2})^2 + 4t^2}}{2} - J'\sigma_{k1}\sigma_{k2}, \quad (14)$$

and for $S_k^z = -1$

$$E_{k14,k15} = \frac{J(\sigma_{k1} + \sigma_{k2})}{2} \pm \frac{\sqrt{J^2(\sigma_{k1} - \sigma_{k2})^2 + 4t^2}}{2} - J'\sigma_{k1}\sigma_{k2}. \quad (15)$$

It is evident that the energy spectrum for the particular case with three mobile electrons per decorating dimer is identical to the particular case with one electron per decorating dimer. This reflects the particle-hole symmetry of the present model.

(e) The subspace with $n_k = 4$.

Owing to the particle-hole symmetry, the system with $n_k = 4$ is equivalent to the system without any electron. For this reason, the last eigenvalue for $n_k = 4$ reads $E_{k16} = -J'\sigma_{k1}\sigma_{k2}$.

The sixteen eigenvalues can be straightforwardly used for the calculation of the bond grand-partition function Ξ_k . After tracing out the degrees of freedom of mobile electrons, the bond grand-partition function Ξ_k depends only on the spin states of localized Ising spins, and one may employ the generalized decoration-iteration transformation [33, 34, 52]

$$\begin{aligned} \Xi_k &= \sum_{i=1}^{16} \exp(-\beta E_{ki}) \exp[\beta \mu n_k(E_{ki})] \\ &= \exp(\beta J'\sigma_{k1}\sigma_{k2}) \left\{ 1 + 4 \cosh \left[\frac{\beta J}{2}(\sigma_{k1} + \sigma_{k2}) \right] \right\} \end{aligned}$$

$$\begin{aligned}
& \times \cosh \left[\frac{\beta}{2} \sqrt{J^2(\sigma_{k1} - \sigma_{k2})^2 + 4t^2} \right] (z + z^3) \\
& + 2z^2 \{ 1 + \cosh [\beta J(\sigma_{k1} + \sigma_{k2})] \\
& + \cosh [\beta \sqrt{J^2(\sigma_{k1} - \sigma_{k2})^2 + 4t^2}] \} + z^4 \} \\
& = A \exp(\beta R \sigma_{k1} \sigma_{k2}), \tag{16}
\end{aligned}$$

where $z = \exp(\beta\mu)$ is the fugacity of the mobile electrons. The mapping parameters A and R are given by the "self-consistency" condition of the decoration-iteration transformation (16), which must hold for all four combinations of two Ising spins σ_{k1} and σ_{k2} . Using standard mathematical operations, one can obtain the following expressions

$$A = (V_1 V_2)^{1/2}, \quad \beta R = \frac{1}{2} \ln \left(\frac{V_1}{V_2} \right) + \beta J', \tag{17}$$

where

$$\begin{aligned}
V_1 &= 1 + 4(z + z^3) \cosh(\beta J) \cosh(\beta t) \\
&+ 2z^2 [1 + \cosh(2\beta J) + \cosh(2\beta t)] + z^4, \\
V_2 &= 1 + 4(z + z^3) \cosh(\beta \sqrt{J^2 + t^2}) \\
&+ 2z^2 [2 + \cosh(2\beta \sqrt{J^2 + t^2})] + z^4. \tag{18}
\end{aligned}$$

By a straightforward substitution of the generalized decoration-iteration transformation (16) into the expression (3), one obtains a simple mapping relation between the grand-canonical partition function Ξ of the interacting spin-electron system on doubly decorated 2D lattices and, respectively, the canonical partition function Z_{IM} of a simple spin-1/2 Ising model on the corresponding undecorated lattice with an effective nearest-neighbour interaction R

$$\Xi(\beta, J, J', t) = A^{Nq/2} Z_{IM}(\beta, R). \tag{19}$$

The mapping parameter A cannot cause a non-analytic behaviour of the grand-canonical partition function Ξ and thus, the investigated spin-electron system becomes critical if and only if the corresponding Ising model becomes critical as well. The average number of mobile electrons per decorating dimer is given by

$$\begin{aligned}
\rho &= \langle n_k \rangle = \frac{z}{N} \frac{\partial}{\partial z} \ln \Xi = z \frac{\partial}{\partial z} \ln A + z \varepsilon \frac{\partial}{\partial z} \beta R \\
&= \frac{z}{2} \left(\frac{V_1'}{V_1} + \frac{V_2'}{V_2} \right) + \frac{z}{2} \varepsilon \left(\frac{V_1'}{V_1} - \frac{V_2'}{V_2} \right), \tag{20}
\end{aligned}$$

where

$$\begin{aligned}
V_1' &= \frac{\partial V_1}{\partial z} = 4(1 + 3z^2) \cosh(\beta J) \cosh(\beta t) \\
&+ 4z [1 + \cosh(2\beta J) + \cosh(2\beta t)] + 4z^3, \\
V_2' &= \frac{\partial V_2}{\partial z} = 4(1 + 3z^2) \cosh(\beta \sqrt{J^2 + t^2}) \\
&+ 4z [2 + \cosh(2\beta \sqrt{J^2 + t^2})] + 4z^3. \tag{21}
\end{aligned}$$

The critical points of the coupled spin-electron system on doubly decorated 2D lattices can now be obtained from the expression (20) for the average number of mobile electrons after

taking into account the critical value of the nearest-neighbour pair correlation function $\varepsilon = \langle \sigma_{k1} \sigma_{k2} \rangle$ of the effective spin-1/2 Ising model along with the critical value of the effective coupling $\beta_c R$. Critical values of the effective coupling $\beta_c R$ and nearest-neighbour pair correlation functions ε_c of the spin-1/2 Ising model on a few different 2D lattices are listed in Tab. 1. It is generally known that the critical values for the *AF* Ising

lattice type	$\beta_c R$	ε_c^F
honeycomb	$\pm \frac{1}{2} \ln(2 + \sqrt{3})$	$\pm 4\sqrt{3}/9$
square	$\pm \frac{1}{2} \ln(1 + \sqrt{2})$	$\pm 1/\sqrt{2}$
kagome	$\frac{1}{4} \ln(3 + 2\sqrt{3})$	$(1 + 2\sqrt{3})/6$
triangular	$\frac{1}{4} \ln 3$	$2/3$
diced	$\pm \frac{1}{2} \ln \left[\frac{1}{2} (1 + \sqrt{3} + \sqrt[4]{12}) \right]$	$\pm \frac{1}{3^{3/4}} (\sqrt{2/3} + 1/\sqrt{2})$

Table 1: Critical parameters for a few different planar Ising lattices with spin ± 1 . The \pm sign corresponds to the *F*(+)/*AF*(-) model.

model are the same (but of opposite signs) as for the *F* ones on loose-packed lattices (e.g. honeycomb and square), while the *AF* Ising models on the close-packed lattices (like the triangular and kagome lattice) cannot exhibit criticality at non-zero temperatures.

The mapping relation (19) between the partition functions allows us to study also thermodynamic quantities, like the grand potential Ω , the internal energy U , the entropy S and the specific heat C using the basic relations

$$\begin{aligned}
\Omega &= -k_B T \ln \Xi, & U &= -\frac{\partial \ln \Xi}{\partial \beta}, \\
S &= -\left(\frac{\partial \Omega}{\partial T} \right)_z, & C &= \frac{\partial U}{\partial T}. \tag{22}
\end{aligned}$$

In addition, we will concentrate our attention on a detailed analysis of the uniform and staggered magnetizations of the localized Ising spins and the mobile electrons, which can serve as order parameters for the *F* and *AF* states, respectively. Applying exact mapping theorems developed by Barry *et al.* [53–56], the magnetization of nodal Ising spins equals to the magnetization of the corresponding spin-1/2 Ising model on the undecorated lattice

$$m_i \equiv \frac{1}{2} \langle \hat{\sigma}_{k1}^z + \hat{\sigma}_{k2}^z \rangle = \frac{1}{2} \langle \hat{\sigma}_{k1}^z + \hat{\sigma}_{k2}^z \rangle_{IM} \equiv m_{IM}. \tag{23}$$

The symbols $\langle \dots \rangle$ and $\langle \dots \rangle_{IM}$ denote the standard ensemble average within the original spin-electron model and the effective Ising model, respectively. The magnetization of the Ising spins can be calculated from the following expressions

$$\begin{aligned}
m_{IM} &= (1 - P)^{1/8}, \\
P &= \begin{cases} \frac{16y^3(1+y^3)}{(1-y)^3(1-y^2)^3} & [57] \text{ (honeycomb)} \\ \frac{16y^4}{(1-y^2)^4} & [58] \text{ (square)} \\ \frac{16y^6}{(1+3y^2)(1-y^2)^3} & [59] \text{ (triangular)}, \end{cases} \tag{24}
\end{aligned}$$

where $y = \exp(-2\beta R)$. The total magnetization of mobile electrons per decorating dimer can be derived from the generalized Callen-Suzuki identity [60, 61]

$$\langle f(\hat{c}_{k\alpha,\gamma}^\dagger \hat{c}_{k\alpha,\gamma}) \rangle = \left\langle \frac{\text{Tr}_k f(\hat{c}_{k\alpha,\gamma}^\dagger \hat{c}_{k\alpha,\gamma}) \exp(-\beta \hat{\mathcal{H}}_k) \exp(\beta \mu \hat{n}_k)}{\text{Tr}_k \exp(-\beta \hat{\mathcal{H}}_k) \exp(\beta \mu \hat{n}_k)} \right\rangle, \quad (25)$$

where $\alpha=1,2$, $\gamma=\uparrow,\downarrow$ and f is an arbitrary function of creation and annihilation operators from the k -th bond Hamiltonian $\hat{\mathcal{H}}_k$. As a result, one obtains the following formula for the magnetization of mobile electrons

$$\begin{aligned} m_e &= \left\langle \sum_{i=1}^2 (n_{ki,\uparrow} - n_{ki,\downarrow}) \right\rangle = \left\langle \frac{1}{\Xi_k} \left[\frac{\partial \Xi_k}{\partial(\beta J \sigma_{k1})} + \frac{\partial \Xi_k}{\partial(\beta J \sigma_{k2})} \right] \right\rangle \\ &= \frac{4m_i}{V_1} \left[(z + z^3) \cosh(\beta t) \sinh(\beta J) + z^2 \sinh(2\beta J) \right]. \end{aligned} \quad (26)$$

It should be noted that the expressions for the spontaneous magnetizations m_i and m_e hold just for the case with the F effective interaction $\beta R > 0$, which supports the existence of the F phase. For the AF effective interaction $\beta R < 0$, it is necessary to calculate new order parameters known as the staggered magnetization of localized Ising spins (m_i^s) and the staggered magnetization of mobile electrons (m_e^s) per decorating dimer. As in the previous case, the staggered magnetization m_i^s can be obtained from the exact mapping theorem

$$m_i^s \equiv \frac{1}{2} \langle \hat{\sigma}_{k1}^z - \hat{\sigma}_{k2}^z \rangle = \frac{1}{2} \langle \hat{\sigma}_{k1}^z - \hat{\sigma}_{k2}^z \rangle_{IM} \equiv m_{IM}^s. \quad (27)$$

Owing to this fact, the staggered magnetization of the localized Ising spins m_i^s has the following explicit form on the honeycomb [57] and square [58] lattices

$$\begin{aligned} m_i^s &= \frac{1}{2} \left[1 - \frac{16x^3(1+x^3)}{(1-x^2)^3(1-x)^3} \right]^{1/8}, \quad (\text{honeycomb}) \\ m_i^s &= \frac{1}{2} \left[1 - \frac{16x^4}{(1-x^2)^4} \right]^{1/8}, \quad (\text{square}) \end{aligned} \quad (28)$$

where $x = \exp(-2\beta|R|)$. The staggered magnetization m_i^s follows the same formula (28) on the loose-packed lattices as does the uniform magnetization m_i given by Eq. (24), while it becomes identically zero on close-packed lattices due to a lack of spontaneous AF long-range order caused by a geometric spin frustration. The staggered magnetization of mobile electrons can be derived by the use of the Callen-Suzuki identity, which provides for m_e^s the following expression depending on the bond grand-partition function Ξ_k and its derivatives

$$\begin{aligned} m_e^s &= \langle (n_{k1,\uparrow} - n_{k1,\downarrow}) - (n_{k2,\uparrow} - n_{k2,\downarrow}) \rangle \\ &= \left\langle \frac{1}{\Xi_k} \left[\frac{\partial \Xi_k}{\partial(\beta J \sigma_{k1})} - \frac{\partial \Xi_k}{\partial(\beta J \sigma_{k2})} \right] \right\rangle. \end{aligned} \quad (29)$$

After straightforward but cumbersome calculations, one obtains an explicit formula for the staggered magnetization of mobile electrons m_e^s on the 2D doubly decorated lattices

$$\begin{aligned} m_e^s &= \frac{(z + z^3) \sinh(\beta \sqrt{J^2 + t^2}) + z^2 \sinh(2\beta \sqrt{J^2 + t^2})}{V_2 \sqrt{J^2 + t^2}} \\ &\times 4Jm_i^s, \end{aligned} \quad (30)$$

which is expressed in terms of the formerly derived staggered magnetization of the Ising spins m_i^s . Finally, the calculation of the electron compressibility follows from the knowledge of the average electron density ρ according to [62]

$$\kappa = \frac{1}{\rho^2} \left(\frac{\partial \rho}{\partial \mu} \right)_T. \quad (31)$$

The exact expression (20) for the average number of mobile electrons can be now utilized in order to find the following expression for the electron compressibility

$$\begin{aligned} \kappa &= \frac{z}{2} \left\{ \beta \Gamma + \frac{(1+\varepsilon)}{V_1^2} \left[\frac{\partial V_1'}{\partial \mu} V_1 - V_1' \frac{\partial V_1}{\partial \mu} \right] \right. \\ &\quad \left. + \frac{(1-\varepsilon)}{V_2^2} \left[\frac{\partial V_2'}{\partial \mu} V_2 - V_2' \frac{\partial V_2}{\partial \mu} \right] \right\}, \end{aligned} \quad (32)$$

where

$$\Gamma = \left[\frac{V_1'}{V_1} (1+\varepsilon) + \frac{V_2'}{V_2} (1-\varepsilon) \right]. \quad (33)$$

3. Results and discussion

In the following we will provide a detailed discussion of the most interesting results obtained for the extended spin-electron model on doubly decorated planar lattices. First of all, it is worth mentioning that all exact results derived in the previous section remain unchanged under the transformation $J \rightarrow -J$. A change of the F Ising interaction $J > 0$ to the AF one $J < 0$ results in a rather trivial change of the mutual spin orientation of the mobile electrons with respect to their nearest Ising neighbours. Consequently, the critical temperature as well as other thermodynamic quantities (except the sign of order parameters) remain unchanged under the transformation $J \rightarrow -J$ and one may further consider the F interaction $J > 0$ without loss of generality. On the other hand, it should be expected that different types of further-neighbour Ising interaction J' between the localized Ising spins may basically influence the physical properties of the model under investigation. For this reason, we will investigate the model with the F ($J' > 0$) as well as AF ($J' < 0$) further-neighbour Ising interaction in addition to the zero interaction limit ($J' = 0$). Our further discussion of thermodynamic characteristics will be restricted only to the case $\rho \leq 2$ due to the validity of particle-hole symmetry. For simplicity, we will use the magnitude of the nearest-neighbour Ising interaction J between localized spins and mobile electrons as the energy unit when normalizing all other parameters with respect to this coupling.

3.1. Ground state

At first, let us perform an exhaustive study of the ground state of correlated spin-electron system for different values of the relative strength of the further-neighbour interaction J'/J . Our analysis has shown that the competition between the model parameters (μ, J, J' and t) leads to several ground states with different number of mobile electrons per decorating dimer, which may result in qualitatively different ground-state

phase diagrams. It turns out that even small non-zero values of the further-neighbour coupling J'/J strongly influences the ground-state phase diagram by generating new ground states, which are totally absent in the ground-state phase diagram for $J'/J = 0$ (Fig. 2(a)). For better clarity, we have collected the ground-state eigenvectors together with the respective eigenenergies and phase boundaries in Tab. 2. The microscopic nature of the ground states for $J'/J = 0$ has been examined in detail in our preceding work [63] to which the interested readers are referred to for further details. Herewith we will concentrate our attention to the effect of further-neighbour Ising interaction J'/J .

We start our discussion with the particular case with F further-neighbour interaction $J'/J > 0$. It could be expected that the F further-neighbour interaction will stabilize the F phases (the phase I and III) at the expense of the remaining phases (0, II and IV) that may additionally undergo qualitative changes. Indeed, we have found that the eigenvectors of the phases I and III remain qualitative unchanged, whereas the corresponding eigenenergies are only shifted by the constant $-J'$ (see Tab. 2). The ground-state phase diagrams are presented in Fig. 2(b)-(d) for a few selected values of the F further-neighbour interaction $J'/J > 0$. For the ground states 0

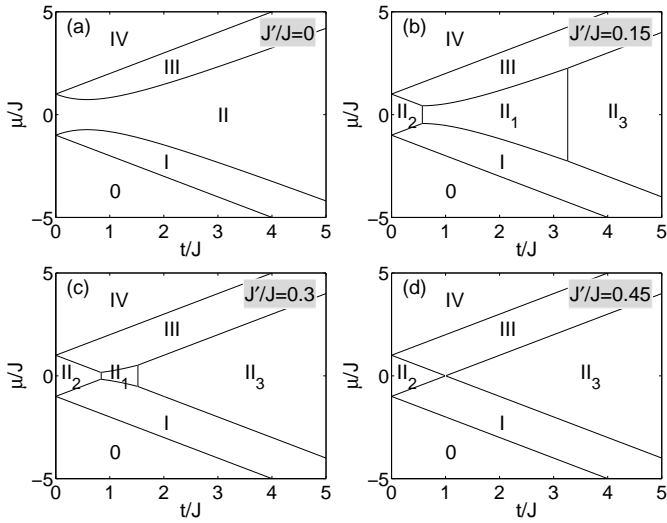


Figure 2: Ground-state phase diagrams of the coupled spin-electron model (1) in the $t/J - \mu/J$ plane for $J'/J = 0$ and the F further-neighbour coupling $J'/J > 0$.

and IV, in which the electron subsystem is empty or fully occupied, the additional F interaction J'/J influences only the spin subsystem. As a result, the F spin alignment of the localized Ising spins is strictly preferred instead of a random spin orientation observed in the ground states 0 and IV on assumption that $J'/J = 0$. The corresponding eigenenergies are therefore shifted only by the constant $-J'$. In the spirit of these facts, it is not surprising that the phase boundaries between phases 0-I and III-IV are identical with the corresponding ones for $J'/J = 0$ (Tab. 2). The situation is much more involved for the ground states with two mobile electrons per decorating dimer, which

cause the AF Néel order II in the limit $J'/J = 0$. Namely, the F interaction J'/J competes with the AF arrangement of the localized Ising spins and it thus strongly influences both subsystems. While the classical F spin arrangement between the localized Ising spins and the mobile electrons is preferred within the phase II₂ emerging for sufficiently small values of the hopping term $t < \sqrt{2JJ'} + J'^2$, the quantum superposition of two AF and two non-magnetic ionic states of the mobile electrons accompanies a perfect F alignment of the localized Ising spins within the ground state II₃ for strong enough hopping amplitudes for $t > (J^2 - J'^2)/2J'$ (see Tab. 2). These two novel ground states become dominant with increasing J'/J until the AF Néel ground state II₁ completely disappears from the ground-state phase diagram. Nevertheless, all three phases coexist together at the appropriate small values of J'/J . Thus, we can conclude that the variation of the kinetic term may lead to a magnetic phase transition, while the number of mobile electrons is kept constant. On the other hand, the AF further-neighbour interaction $J'/J < 0$ should stabilize the AF phase (the phase II) at the expense of the remaining ground states (0, I, III and IV), as it is illustrated in Fig. 3. It actually turns out that the ground

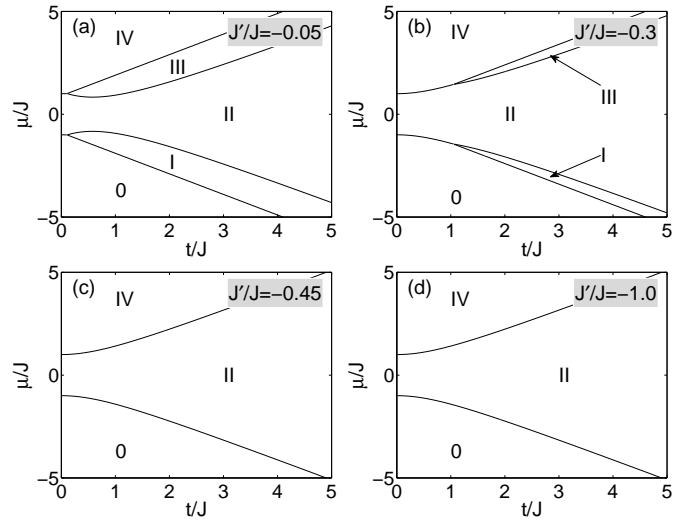


Figure 3: Ground-state phase diagrams of the extended spin-electron model (1) in the $t/J - \mu/J$ plane for the AF further-neighbour coupling $J'/J < 0$.

state II with two mobile electrons per decorating dimer cannot be accompanied with the F alignment of localized Ising spins, which originate in the phases II₂ and II₃ exclusively from the F further-neighbour interaction (the hopping process of two mobile electrons transmits an effective AF interaction between the localized Ising spins). Bearing this in mind, the AF further-neighbour interaction does not alter the ground state II with two mobile electrons per decorating dimer, which still exhibits the quantum Néel ordering with a perfect AF arrangement of localized Ising spins and the quantum AF arrangement of the mobile electrons underlying a quantum superposition of two AF and two non-magnetic states. The corresponding eigenenergy of the phase II has the similar form with a rather trivial extension by

the further-neighbour interaction $+|J'|$ (see Tab. 2). Similarly as for $J'/J > 0$, the AF further-neighbour interaction J'/J influences only the spin subsystem of the phase 0 and IV with an empty or fully occupied electron subsystem, where the classical Néel long-range order of the localized Ising spins is preferred and the corresponding eigenenergies are only shifted by the constant $-J'$. Surprisingly, the AF further-neighbour interaction still favors the same arrangement of the electron as well as spin subsystems as for the case $J'/J = 0$ for the ground states I and III with one and three electrons per decorating dimer. When the hopping term is sufficiently weak $t < -2J'[(J+J')/(J+2J')]$ with respect to the AF further-neighbour interaction J' , the ground states with odd number of mobile electrons per dimer are suppressed by the quantum AF ground state II with two electrons per decorating dimer. The ground-state phase diagram consists only of phases with an even number of mobile electrons per dimer if $\left[-(1+t/J) - \sqrt{(t/J)^2 + 1} \right] / 2 < J'/J < \left[-(1+t/J) + \sqrt{(t/J)^2 + 1} \right] / 2$, as is illustrated in Fig. 3(d).

3.2. Finite-temperature phase diagrams

It has been demonstrated in our previous works [46, 63] that the finite-temperature phase diagram of the coupled spin-electron model on doubly decorated 2D lattices displays similar features for several lattice topologies. Therefore our further discussion will be restricted only to the representative case of the double decorated square lattice. Fig. 4 illustrates a few typical finite-temperature phase diagrams in the form of critical temperature versus electron concentration plots for several values of the F further-neighbour coupling $J'/J > 0$.

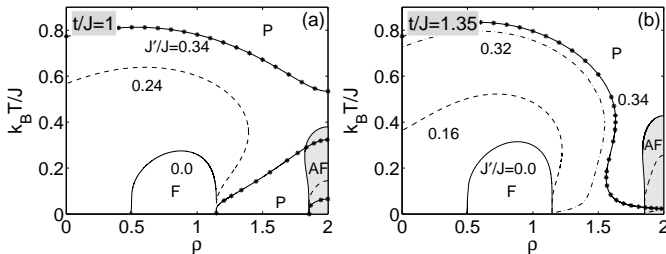


Figure 4: Phase diagrams in the $\rho - k_B T/J$ plane for two representative values of t/J ($t/J = 1$ and 1.35) and distinct F further-neighbour interaction J'/J . Different lines illustrate the borders between the AF - P and F - P phases. The shaded area has been used for the better visualization of the AF phase.

It is evident that the area corresponding to the F long-range order (in the vicinity of $\rho \approx 1$) generally increases with increasing J'/J , whereas the area corresponding to the AF state (in the vicinity of $\rho \approx 2$) gradually diminishes. The most pronounced changes in the phase diagram can be primarily observed at low electron concentrations, where the spontaneous F long-range order appears due to the non-zero further-neighbour interaction $J'/J \neq 0$ also below the bond percolation threshold $\rho = 0.5$, in contrast with the particular case of $J'/J = 0$. In addition, there exists a critical value of J'/J above which only the F state can

be detected for all possible electron concentrations ρ (e.g., see the curve $J'/J=0.34$ in Fig. 4(b)). As far as the reentrant transitions are concerned, we have found that the F further-neighbour interaction $J'/J > 0$ may produce many types of magnetic reentrant phenomena, some of which are absent in the model with $J'/J = 0$. If the further-neighbour coupling is weaker than $J'/J \approx 0.05$, the system exhibits a reentrant phase transitions with two consecutive critical points similar to the ones observed for $J'/J = 0$ for both the F and AF phases. The reentrant phase transitions with two consecutive critical points can be also observed for $J'/J \geq 0.05$, but only for the F case. Moreover for the higher further-neighbour interaction ($J'/J \gtrsim 0.08$), a different mechanism underlines their formation, as illustrated in Fig. 5. Surprisingly, the temperature fluctuations support an ap-

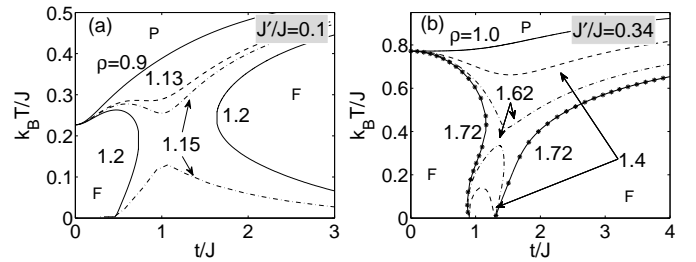


Figure 5: Phase diagrams in the $t/J - k_B T/J$ plane for a few selected values of J'/J and ρ corresponding to the F phase. Different lines illustrate the borders between the F and P phase. For $\rho = 1.15$ in the panel (a) and $\rho = 1.4$ and 1.62 in the panel (b) the F phase is delimited by border lines, above and below which the P phase occurs.

pearance of the F long-range order above the P ground state when the hopping integral t is smaller or greater than the Ising coupling and the electron filling $\rho \gtrsim 1$, see Fig. 5(a). The F state then persists in a rather narrow temperature interval. A further temperature increase destroys this state. It was found that the P - F - P reentrance observed for $t/J > 1$ is markedly reduced for a stronger further-neighbour interaction ($J'/J \gtrsim 0.2$) and the system exhibits a single transition from the F to the P state, as seen Fig. 5(b). As one can see from Fig. 5(b), a sufficiently strong further-neighbour F coupling is responsible for the existence of other reentrant phase transitions with three consecutive critical points, namely F - P - F - P , near the electron filling $\rho \approx 1.5$, e.g., for $\rho = 1.62$. Last but not least, new reentrant phenomena produced by the non-zero F further-neighbour interaction are the mixed reentrant phase transitions with three consecutive critical points of the AF - P - F - P type. The term mixed reentrant phase transition is used to denote the situation when the investigated model system re-enters at higher temperatures to a spontaneous ordering of another type than at lower temperatures. Such behaviour exists only near the half-filled band case ($\rho \approx 2$) and appropriate model parameters $t/J \approx 1$ and $J'/J \approx 1/3$ (see border lines for $J'/J = 0.34$ in Fig. 4(a)). It is clear that this behaviour is a direct effect of the additional further-neighbour Ising interaction J'/J , because its existence cannot be observed for the $J'/J = 0$.

The obtained phase diagrams are more complex for the AF further-neighbour interaction $J'/J < 0$. In Fig. 6 we present

a few typical finite-temperature phase diagrams for two representative values of the hopping term $t/J = 0.25$ and 1 . It is evident that the AF further-neighbour interaction between the localized Ising spins reduces the critical temperature of the F phase (in the vicinity of $\rho \approx 1$) and increases (in comparison with the $J'/J = 0$) the lower critical concentration (up to $\rho_c = 0.854$) of the mobile electrons needed for the onset of the F long-range order at relatively low temperatures. Moreover, the small additional AF further-neighbour interaction generates a new $P-F-P$ reentrant transition for smaller electron concentrations $\rho < 1$. Even though the F long-range order is generally

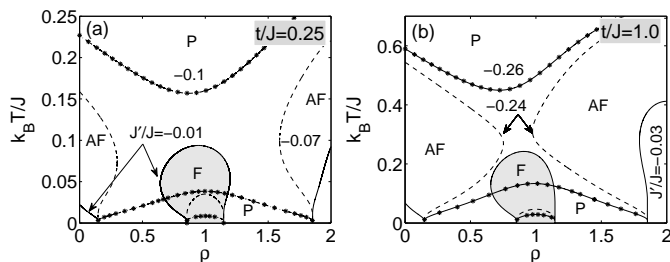


Figure 6: Phase diagrams in the $\rho - k_B T/J$ plane for two representative values of t/J calculated for $J'/J < 0$. Different lines illustrate the borders between the AF - P and F - P phases. The shaded area has been used for the better visualization of the F phase.

reduced with the AF further-neighbour interaction J'/J , the F long-range order still ends up at the same upper critical concentration $\rho_c^U = 1.146$ as for $J'/J = 0$. Contrary to this, the AF phase gradually fills up the whole region of the phase diagram, because the new AF phase emerges at small electron concentrations $\rho \rightarrow 0$. Both AF phases are stabilized through the AF further-neighbour interaction $J'/J < 0$ and are subsequently connected into one large common AF area above a certain threshold value. Also for the AF further-neighbour interactions $J'/J < 0$, the interesting mixed reentrant sequence of transitions F - P - AF - P has been detected. Contrary to the former case with $J'/J > 0$, where similar reentrant transitions AF - P - F - P occurs just for the electron concentrations close to a half-filling $\rho \approx 2$, the reentrant transitions F - P - AF - P can be observed only for electron concentrations in the vicinity of $\rho \approx 1$. This effect is also a direct consequence of the additional further-neighbor Ising interaction J'/J , because its existence cannot be observed for $J'/J = 0$.

3.3. The magnetization, specific heat and compressibility

The existence of mixed reentrant transitions motivated us to investigate also the behaviour of selected physical quantities, e.g., the magnetizations, specific heat and compressibility with the goal to provide a more complete understanding of the considered coupled spin-electron system. We start our discussion with the particular case with a F further-neighbour interaction $J'/J > 0$ at half-filling $\rho = 2$. If the additional further-neighbour interaction is relatively small, the system should exhibit the AF long-range order at low enough temperatures and the disordered P phase at higher temperatures. The spontaneous

staggered magnetizations m_i^s and m_e^s of the localized Ising spins and mobile electrons shown in Fig. 7(a) indeed confirm the AF nature of both spin as well as electron subsystems. The mag-

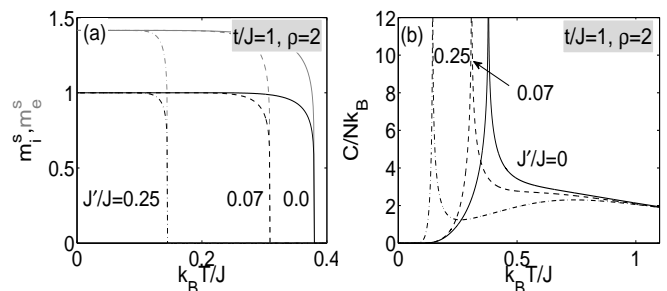


Figure 7: The staggered magnetizations m_i^s (black lines) and m_e^s (gray lines) and corresponding specific heat as a function of temperature for $t/J = 1$, $\rho = 2$ and $J'/J \geq 0$ generating the AF state.

netic moment of localized Ising spins exhibits a perfect Néel long-range order characterized by the maximal value of $m_i^s = 1$ at zero temperature. On the other hand, the quantum fluctuations present in the electron subsystem lead to a quantum reduction of the staggered magnetization of mobile electrons m_e^s . For this reason, the saturation value of m_e^s is not equal to its maximal value, but reaches the value $2/\sqrt{1+(t/J)^2}$. Both staggered magnetizations remain nearly constant as temperature increases up to moderate temperatures. Then they rapidly vanish in the vicinity of the critical temperature with the identical critical exponent $\beta_m = 1/8$ from the standard Ising universality class. It is evident from Fig. 7(a) that the critical temperature declines upon strengthening of the F further-neighbour coupling J'/J . The significant changes in the magnetization curves are also reflected in the specific heat, where a relatively narrow sharp but still finite maximum (cusp) is observed at the critical temperature for both non-integer and integer electron concentrations. The previously conjectured possibility of a logarithmic divergence of the specific heat for integer average electron concentrations [63] has been ruled out by more accurate numerical calculations with the temperature step up to 10^{-9} . The present results definitively confirm the finite character of the narrow sharp maximum of the specific heat also for integer values of electron concentration, as illustrated in Fig. 8. The specific-heat curves may also exhibit an additional broad maximum located at higher temperatures with the dominant contribution from the electron subsystem. The situation is very different for a sufficiently large F further-neighbour coupling J'/J , where only the F long-range order is present, e.g., $J'/J = 0.45$ (see Fig. 9(a)). In this case both uniform magnetizations start from the identical value $m_i = m_e = 1$ and commonly vanish at the critical temperature keeping the critical exponent $\beta_m = 1/8$ identical with the standard Ising universality class. Nevertheless, there is an evident difference in magnetizations at moderate temperatures, where the electron subsystem is more susceptible with respect to temperature fluctuations than the spin subsystem. Also the character of the specific heat is slightly different with a narrow finite cusp, whose position (contrary to the small J'/J) shifts to

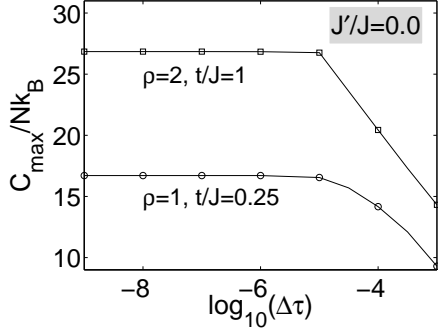


Figure 8: The dependencies of the cusp maximum on the temperature step for integer electron concentrations ($\rho = 1$ and $\rho = 2$) and two representative values of t/J . The lines are the guide for eyes.

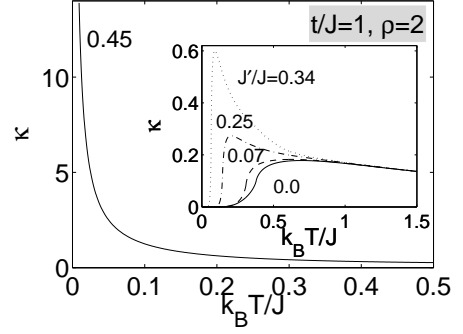


Figure 10: Thermal dependencies of the electron compressibility for a few different values of the F further-neighbour interactions, the electron concentration $\rho = 2$ and the hopping parameter $t/J = 1$.

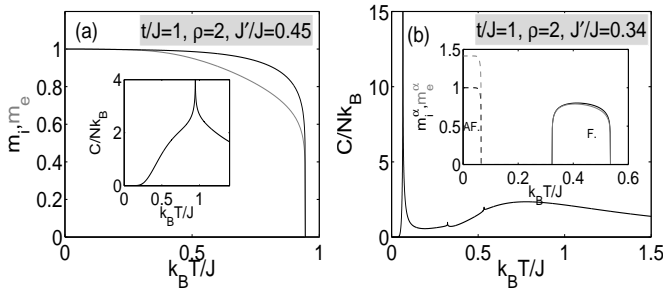


Figure 9: (a) The magnetizations m_i (black lines) and m_e (gray lines) and corresponding specific heat (inset) as a function of temperature for $t/J = 1$, $\rho = 2$ and $J'/J = 0.45$ generating just the F state. (b) The thermal dependence of the specific heat in the case with mixed reentrant transitions $AF-P-F-P$ for $J'/J = 0.34$. Inset: uniform (solid lines) and staggered (dashed lines) magnetizations as a function of temperature for the same model parameters.

a higher temperature and its magnitude becomes smaller. However, the most attractive type of reentrant phase transitions relates to the thermally driven magnetic transition from the AF to the F state through the intermediate P state. Under this circumstance the AF order vanishes at relatively low critical temperature with an identical behaviour of magnetic moments for spin and electron subsystems. Afterwards the F phase becomes favorable at moderate temperatures, which is manifested by a loop character of uniform magnetizations with $m_i \gtrsim m_e$. The specific heat consequently displays an interesting temperature dependence, in which the development or disappearance of spontaneous (uniform or staggered) magnetizations is reflected by finite cusps (Fig. 9(b)). It is found from the analysis of the electron compressibility κ that the system in the AF state exhibits a huge rigidity ($\kappa(0) = 0$), which is generally weakened as the ratio J'/J increases (inset in Fig. 10). An increase in the further-neighbour Ising interaction of the F type leads to the formation of a visible kink connected to the fluctuation of particles, which become more free and destroy the stability of the system. Thus, the magnitude of the kink determines the degree of its compressibility. On the other hand, the transition to the F state ($J'/J = 0.45$ in Fig. 10) due to the further-neighbour J'/J

interaction is accompanied with a rapid divergence of the compressibility, which indicates a reduction of the system's rigidity.

Contrary to the previous case, the AF further-neighbour interaction J'/J reduces the F phase. Owing to this fact, the mechanism of thermally-induced changes in the spontaneous magnetization is different. For a relatively small $|J'/J|$, which is not strong enough to destroy the F ground state, the uniform magnetization of both subsystems starts from the zero-temperature asymptotic value equal to its saturation value provided that the electron concentration is equals to $\rho=1$, as shown in the inset of Fig. 11(a). The specific heat

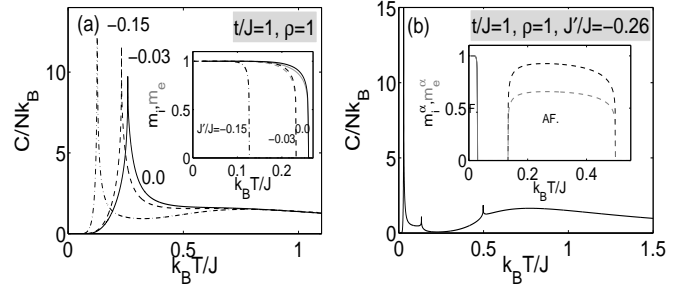


Figure 11: (a) The specific heat and corresponding magnetizations m_i (black lines) or m_e (gray lines) as a function of temperature for $t/J = 1$, $\rho = 1$ and $J'/J < 0$. (b) The thermal dependence of the specific heat in a case with mixed reentrant transitions for $J'/J < 0$. Inset: uniform (solid lines) and staggered (dashed lines) magnetizations as a function of temperature for the same model parameters.

curves show just two separate maxima, one significant finite cusp connected to the order-disorder phase transition and one more or less visible broad maximum whose origin lies predominantly in thermal excitations of the electron subsystem. For the case with mixed reentrant phase transitions $F-P-AF-P$, the uniform spontaneous magnetizations within the F phase decline until they both vanish at the lowest critical temperature. A further temperature increase is responsible for the up rise of the staggered magnetizations within the AF phase with a more interesting loop thermal dependencies with $m_i^s \gtrsim m_e^s$. In accordance with this phenomenology, the corresponding

temperature dependence of the specific heat shows a finite cusp at each critical temperature, where either spontaneous uniform or staggered magnetization disappears, as illustrated in Fig. 11(b). If the *AF* further-neighbour Ising interaction

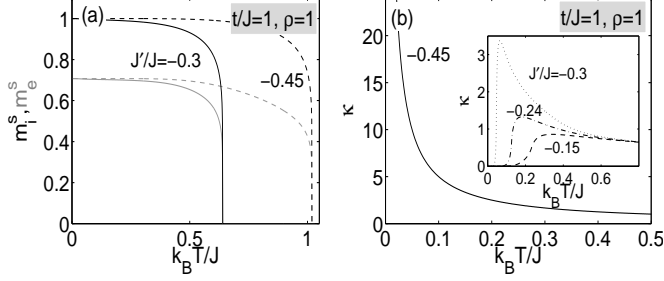


Figure 12: (a) The staggered magnetizations m_i^s (black lines) or m_e^s (gray lines) as a function of temperature for $t/J = 1$, $\rho = 1$ and $J'/J < 0$ producing the *AF* phase. (b) The thermal dependence of the electron compressibility for a few different values of the *AF* further-neighbour interactions, electron concentration $\rho = 1$ and hopping parameter $t/J = 1$.

is sufficiently strong to enforce a perfect Néel arrangement of the localized Ising spins, the staggered magnetizations follow similar trends except that the staggered magnetization of mobile electrons m_e^s does not start from its saturation value in contrast to the staggered magnetization of the localized Ising spins (Fig. 12(a)). The corresponding specific heat has a simple thermal dependence with a single sharp cusp located at the critical point. The electron compressibility of the system (Fig. 12(b)) with *AF* further-neighbour interaction indicates a huge rigidity for the *F* phase with $\kappa = 0$, while large κ values points to a large instability in the *AF* phase.

We have also analyzed other basic thermodynamic characteristics out of mixed reentrant phase transitions. In the following, we will present just the most interesting results to demonstrate the richness of the present model. We start our discussion with the case $J'/J \gtrsim 0$ and high electron concentrations leading to the presence of a spontaneous *AF* arrangement. It will be demonstrated that the increasing temperature influences the behaviour of sublattice magnetizations in a different way. Out of the reentrant regime, the staggered magnetizations of localized Ising spins as well as mobile electrons gradually fall down with increasing temperature until they completely vanish at a critical temperature, as illustrated in Fig. 13(a). However, it should be pointed out that the staggered magnetization m_e^s is higher than the staggered magnetization m_i^s . While the staggered magnetization m_e^s undergoes a quantum reduction, the staggered magnetization m_i^s is substantially reduced by the annealed bond disorder. Also the specific heat displays a more diverse temperature dependence including a sharp finite cusp along with a broad high-temperature maximum sometimes accompanied with another smaller broad maximum. Other types of magnetization curves are connected to the *P* – *AF* – *P* reentrant phase transition (with a loop character) or dependences in their close neighbourhood [see upper curves in the inset of Fig.13(b)]. In this parameter space

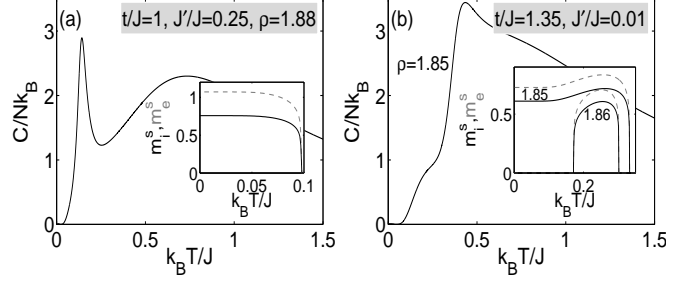


Figure 13: Thermal dependencies of the specific heat for the *AF* phase for $J'/J > 0$, $\rho \rightarrow 2$ and (a) $t/J = 1$ or (b) $t/J = 1.35$. Insets: the respective thermal variations of staggered magnetizations.

region, the specific heat has a simple behaviour, as shown in Fig. 13(b). The influence of the *F* further-neighbour Ising interaction J'/J is very significant, especially on the opposite parameter space with low electron concentrations ($\rho < 1$), where the *F* further-neighbour Ising interaction stabilize the *F* phase. For $J'/J \gtrsim 0$, the localized Ising spins display a perfect spontaneous *F* ordering with $m_i \equiv 1$, quite similarly as the electron subsystem does ($m_e \equiv \rho$). However, temperature fluctuations cause a rather steep decrease of the spontaneous magnetizations of localized Ising spins (see Fig. 14(a)). The

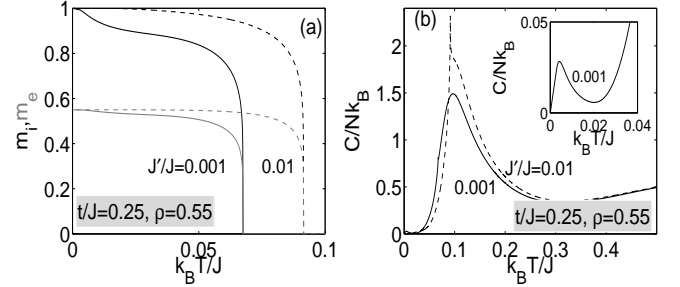


Figure 14: (a) Thermal dependencies of spontaneous magnetizations m_i (black lines) and m_e (gray lines); (b) Thermal dependencies of the specific heat for the *F* phase.

increasing strength of the further-neighbour interaction J'/J reduces the effect of thermal fluctuations and the spontaneous magnetizations persist at their maximum values up to higher temperatures. The specific heat displays for this particular case a broad high-temperature maximum, originating predominantly from thermal excitations of the electron subsystem, and an additional sharp cusp singularity, arising out from both spin and electron subsystems, Fig. 14(b). Note, furthermore, that the specific heat exhibits another low-temperature maximum (inset in Fig. 14(b)) for $J'/J \rightarrow 0$ with a very small height. Such low-temperature maximum is missing in the model without the further-neighbour coupling $J'/J = 0$, so its presence can be attributed to the Ising subsystem. For electron concentrations above a quarter-filling, the thermal variation of the spontaneous magnetization can be divided into two groups, namely, with or without reentrant phase transitions. The reentrant transitions

manifest themselves in the corresponding magnetizations as loop dependencies. Depending on the hopping amplitude, the spontaneous magnetization of mobile electrons m_e can reach higher ($t/J < 1$) or smaller ($t/J \geq 1$) values than the spontaneous magnetization of localized spins m_i , as it is shown in Fig. 15. Comparing this observation with the $J'/J = 0$ case, it is plausible to suppose that the change of the relationship between m_i and m_e is a direct consequence of the further-neighbour interaction J'/J .

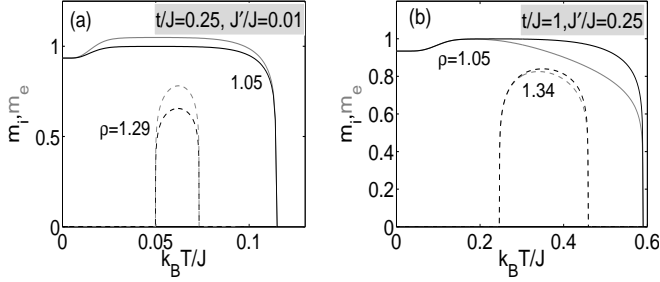


Figure 15: Thermal dependencies of spontaneous magnetizations m_i (black lines) and m_e (gray lines) in the F phase for $\rho > 1$ and (a) $t/J < 1$, (b) $t/J \geq 1$.

Out of the reentrant regime, it is evident that the spontaneous magnetizations are reduced by the annealed bond disorder of the decorating dimers caused by fractional electron concentrations. The disorder can be partially lifted by a non-zero temperature whose increase leads to an almost ideal ferromagnetic alignment of magnetic moments. Of course, both magnetizations vanish together at the critical point, where thermal fluctuations become too large. The region with $t/J \approx 1.35$ exhibits a very interesting diversity of temperature variations of the spontaneous magnetizations, as reported in Fig. 16. It should be stressed that the F state is detected for

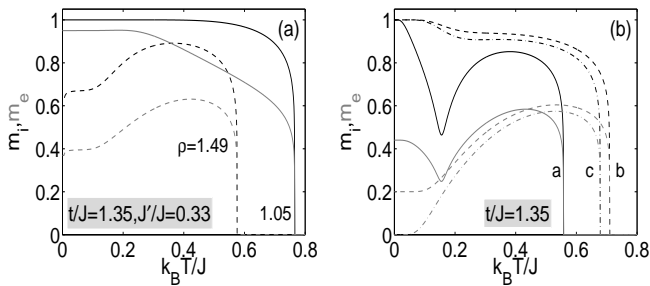


Figure 16: Thermal dependencies of spontaneous magnetizations m_i (black lines) and m_e (gray lines) for $J'/J > 0$, $t/J = 1.35$ and various model parameters. The letters in figure (b) denote the following model parameters a: $J'/J = 0.34$, $\rho = 1.56$, b: $J'/J = 0.4$, $\rho = 1.8$ and c: $J'/J = 0.4$, $\rho = 2$.

all electron concentrations ρ owing to a relatively strong F further-neighbour coupling J'/J , which causes the F alignment of the localized Ising spins even though the spontaneous alignment of mobile electrons is incomplete. It can be seen from

Fig. 16 that increasing temperature diminishes the differences between both sublattice magnetizations, which merge together at the critical point.

The thermal variation of the specific heat in the parameter space with the electron concentration above quarter-filling is also rich. In Fig. 17, we present some typical curves obtained for different model parameters. In general, all specific heats have the multipeak structure with a more or less visible broad high-temperature maximum, which is predominantly formed by the contribution of the electron subsystem accompanied with one or more narrow finite-cusp singularities connected with continuous order-disorder phase transitions. The

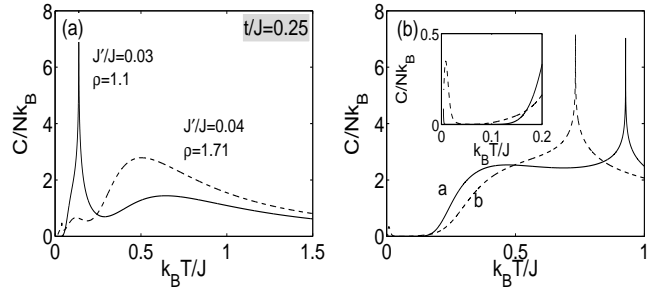


Figure 17: Thermal dependencies of the specific heat for $J'/J > 0$, $\rho > 1$ and selected values of model parameters. Different letters in figure (b) correspond to different model parameters. a: $t/J = 1$, $J'/J = 0.41$, $\rho = 1.05$ and b: $t/J = 1.35$, $J'/J = 0.32$, $\rho = 1.1$.

most fascinating behaviour of the specific heat has been detected near quarter-filling provided that the hopping integral is sufficiently large ($t/J \geq 1$) and the further-neighbour Ising interaction $J'/J > 0$ leads to almost perfect spontaneous F order of all magnetic moments (e.g., for $t/J = 1$, $J'/J = 0.41$ or $t/J = 1.35$, $J'/J = 0.32$ in Fig. 17(b)). Under this condition, the specific heat exhibits a small narrow maximum at very low temperature rapidly falling down almost to zero (inset in Fig. 17(b)), with a further temperature rise. The specific heat do not reach zero value within this interval of moderate temperatures, but it is very small (of the order $10^{-4} - 10^{-5}$). The analysis of the electron compressibility showed that all F phases generated by the F further-neighbour interaction below $\rho < 1$ always exhibit a weak system stability characterized by a rapid divergence of κ (e.g., $\rho = 0.9$, $t/J = 0.25$ and $J'/J = 0.001$ in Fig. 18(a)). On the other hand, the electron compressibility for the F phase at $\rho \geq 1$ shows a huge system rigidity, which basically depends on all other parameters. The system rigidity in the F phase for $\rho \geq 1$ is quite reduced at sufficiently large J'/J , for which the F phase fills up the whole phase diagram. In the AF phase, the electron compressibility always tends to zero for very low temperatures, indicating the huge system rigidity. However, the F further-neighbour interaction rapidly reduces this phase.

Let us turn our attention to the case $J'/J < 0$. It is evident from the phase diagrams shown in Fig. 6 that the AF further-neighbour interaction J'/J stabilizes the AF phase, and constrains the F one. For this reason, let us firstly analyze the F

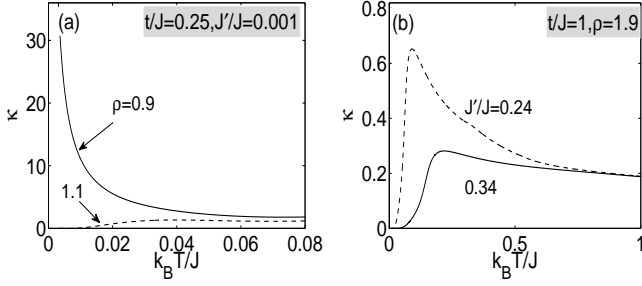


Figure 18: The electron compressibility as a function of temperature for the F further-neighbour interaction and different model parameters.

phase. If the AF further-neighbour interaction is sufficiently

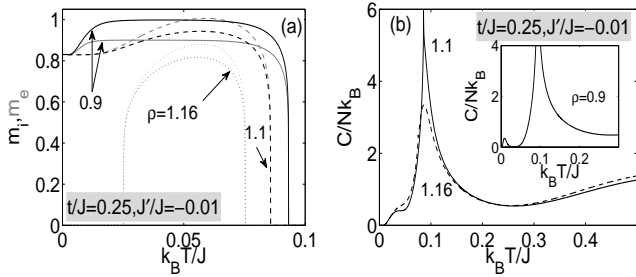


Figure 19: (a) Thermal dependencies of spontaneous magnetizations m_i (black lines) and m_e (gray lines); (b) Thermal dependencies of the corresponding specific heat.

small and the system exhibits a reentrant phase transition in the F phase, the character of the spontaneous magnetizations m_i and m_e is influenced by the electron concentration ρ . Typical examples are presented in Fig. 19(a). As one could expect, the loop behaviour of both magnetizations has been detected for electron concentrations near the lower and upper percolation thresholds connected to the reentrant phase transitions (e.g., $\rho = 1.16$). Between these borders, both spontaneous magnetizations are reduced by the annealed bond disorder, presented at non-zero temperatures (e.g., $\rho = 0.9$ or 1.1) and then commonly vanish at the critical point. It is interesting to note that this reduction is fully absent for very small values of the further-neighbour interaction $|J'/J| \rightarrow 0$ (e.g., $J'/J = -0.001$) where an almost constant behaviour of the uniform magnetizations has been observed at low temperatures. For the higher value of $|J'/J|$, where reentrant transitions in the F phase are absent, both spontaneous magnetizations m_i and m_e are almost indistinguishable functions, whereas the electron concentration influences only the critical temperature as well as their saturation value. Moreover, our analysis shows that for $t/J > 1$ the magnetization of mobile electrons is always smaller than the magnetization of localized spins. However, in the opposite limit $t/J < 1$, such behaviour is observed only for $\rho \lesssim 1$. A slightly different picture has been detected for the special case $t/J = 1$, where reentrant transitions are present only for $\rho \leq 1$. For this parameter set, a behaviour similar to the one described

above for $t/J = 0.25$ and $J'/J = -0.01$ has been observed. On the other hand, both magnetizations are almost indistinguishable for $\rho \geq 1$ and arbitrary J'/J . The thermal variation of the specific heat is very similar to the ones observed for $J'/J > 0$ (see Fig. 19(b)). In general, the specific heat may exhibit a multipeak structure with a broad high-temperature maximum accompanied with relatively narrow finite cusps associated with the formation of spontaneous long-range order.

The spontaneous staggered magnetizations in the AF phase may also show some peculiar features. Depending on the model

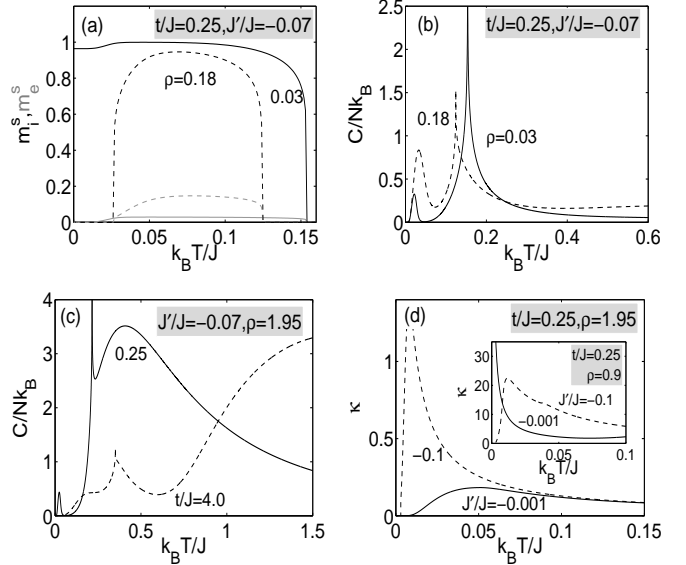


Figure 20: Thermal dependencies of staggered magnetizations (a), specific heat (b)-(c) and electron compressibility (d) for $J'/J < 0$ for different model parameters. Inset: The electron compressibility for the F state and different AF further-neighbour interaction.

parameters one can observe staggered magnetizations with or without a loop character, whereas the staggered magnetization of the mobile electrons does not saturate neither at zero temperature. In general, the electron concentration determines whether $m_i^s > m_e^s$ holds or vice versa. However, the AF further-neighbour coupling $J'/J < 0$ is responsible for the existence of a spontaneous AF long-range order also for small electron concentrations. In this region, the spontaneous order due to the electron subsystem is marginal on account of $m_e^s \rightarrow 0$ (Fig. 20(a)). Contrary to this, the specific heat shows that the electron subsystem has a major influence on the low temperature behaviour. The specific heat exhibits two significant peaks, which arise from the superposition of both subsystem contributions (Fig. 20(b)). Other types of magnetization dependencies were observed for sufficiently large $|J'/J|$ where the AF ground state dominates for all electron concentrations ρ . Namely, the localized Ising spins display a perfect spontaneous Néel order with the saturated staggered magnetization $m_i^s \equiv 1$, while the staggered magnetization of the mobile electron obey a quantum reduction $m_e^s \equiv \rho / \sqrt{1 + (t/J)^2}$. The increasing temperature gradually destroys the AF long-range order due to the mutual

interplay of thermal fluctuations and annealed bond disorder. Fig. 20(c) illustrates a few typical thermal variations of specific heat for the special case without mixed reentrant phase transitions. The strong influence of $J'/J < 0$ has been also observed on the relative magnitude of the electron compressibility κ . While the electron compressibility of the AF state reaches zero at $T = 0$ for an arbitrary $|J'|/J$ [as illustrated in Fig. 20(d)], the electron compressibility of the F state depends basically on the further-neighbour interaction $|J'|/J$ and electron concentration ρ . For $\rho \geq 1$ and arbitrary $|J'|/J$, its character is similar to the AF one, while the electron compressibility diverges below this value for small $|J'|/J$. A decrease in the further-neighbour coupling changes this behaviour and the electron compressibility tends to zero at zero absolute temperature (see inset in Fig. 20(d)).

4. Conclusion

In the present work we analyzed the thermodynamic behavior of an interacting spin-electron system with a variable electron filling on decorating positions of doubly decorated planar lattices by adapting the exact solution based on a generalized decoration-iteration transformation. Besides the hopping integral t and the nearest-neighbour exchange interaction J , we have taken into account an additional further-neighbour exchange interaction between the nodal Ising spins J' . The ground-state analysis as well as thermodynamic study have been performed for the F and AF further-neighbour interactions. It has been shown that the ground-state phase diagrams strongly depend on the type of further-neighbour interaction. As expected, the non-zero value of further-neighbour coupling changes the P phase (detected for $J'/J = 0$) to spontaneously long-range ordered F or AF phases with respect to the type of the further-neighbour interaction. The AF further-neighbour interaction stabilizes the AF phase, while the F one produces two new phases determined by the value of t/J . If the hopping term of the mobile electrons is smaller than the nearest-neighbour interaction ($t/J < 1$), the electron subsystem always prefers an electron distribution with one parallel oriented electron per each decorating site with respect to its neighbouring Ising spin. In the opposite limit ($t/J > 1$), the electron distribution is not fundamentally influenced even though the localized Ising spins change their orientation to the parallel one. It has been found from our analysis that these two new phases become dominant in the phase diagram for the F regime with relatively large J'/J with a complete absence of the AF phase.

Our special interest has been devoted to reentrant phase transitions, which represent a highly debated problem at present. The reentrant phase transitions were observed and investigated in a variety of different physical systems, e.g., binary liquid mixtures [64, 65], spin glasses [66], superconductors [33], liquid crystals [67] and intermetallic compounds [68, 69]. It is known that different intermetallic rare-earth compounds can produce different types of magnetic reentrant transitions [69]. For example, the manganese subsystem of the RMn_2Ge_2 ($R = \text{Pr, Nd}$) compounds undergoes at first a transition from the P

to an AF state and then to the F one with decreasing temperature for light rare earths, e.g., Pr or Nd. On the other hand, $SmMn_2Ge_2$ compound exhibits a phase transition from the P to the AF state and then from the AF to the F state as the temperature is lowered. It is evident that the spectrum of the magnetic reentrant transitions is very rich and theoretical models for a description of this remarkable phenomenon are therefore highly desirable.

In our previous work [63] we have introduced a relative simple model describing the physics of the interacting many-body system composed of the localized Ising spins and mobile electrons. In spite of some simplifications, the model surprisingly described the existence of the reentrant behaviour, separately for the F or AF state. However, the model has not been able to explain an existence of mixed reentrant phase transitions (from the AF through the P state to the F state or vice versa) as found in many rare-earth compounds. Nevertheless, it was shown in the present paper that a little modification of this model, namely taking into consideration the further-neighbour interaction between the localized Ising spins, can also describe the above mentioned mixed reentrant phase transitions. Indeed, a few novel types of reentrant transitions have been determined upon the value of the electron concentration ρ . The non-zero value of the further-neighbour interaction can produce unique reentrant transitions with three consecutive critical points, namely $AF - P - F - P$ for $J'/J > 0$ and $\rho \approx 2$ or $F - P - AF - P$ for $J'/J < 0$ and $\rho \approx 1$, which has been detected as an effect of the additional further-neighbour Ising interaction J'/J and cannot be observed for $J'/J = 0$. Due to the annealed nature of the electron distribution, the specific heat presents finite-cusp singularities at the critical temperature, both for integer-valued as well as fractional electron concentrations. Finally, the obtained result unveiled a competition between the hopping integral, the Ising interaction between nearest-neighbour Ising spin and mobile electrons and the further-neighbour AF interaction between the localized Ising spins. As a result, a rich variety of temperature dependencies of magnetization and specific heat have been presented for the coupled spin-electron system under investigation, whereas many of them are quite reminiscent of that observed experimentally in various magnetic systems (e.g. intermetallic compounds [68–70]). In addition, it has turned out that the critical exponents are from the standard Ising universality class except that for the specific heat, which always shows at a phase transition a finite cusp instead of logarithmic divergence.

This work was supported by the Slovak Research and Development Agency (APVV) under Grant APVV-0097-12 and ERDF EU Grant under the contract No. ITMS26110230097 and No. ITMS26220120005. Partial financial support from the Brazilian agencies CAPES (Coordenação de Aperfeiçoamento de Pessoal de Nível Superior) and CNPq (Conselho Nacional de Desenvolvimento Científico e Tecnológico) is also acknowledged.

References

- [1] D. B. McWhan, A. Menth, J. P. Remeika, W. F. Brinkman, and T. M. Rice, *Phys. Rev. B* **7** (1973) 1920.
- [2] R. von Helmolt, J. Wecker, B. Holzapfel, L. Schultz, and K. Samwer, *Phys. Rev. Lett.* **71** (1993) 2331.
- [3] K. Chahara, T. Ohno, M. Kasai, and Y. Kozono, *Appl. Phys. Lett.* **63** (1993) 1990.
- [4] P. Schiffer, A. P. Ramirez, W. Bao, and S. W. Cheong, *Phys. Rev. Lett.* **75** (1995) 3336.
- [5] P. Wachter, in K. A. Gschneider, L. R. Eyring (Eds.), *Handbook on the Physics and Chemistry of Rare Earths*, vol. 19 North-Holland, Amsterdam (1994).
- [6] J. Kanamori, *Prog. Theor. Phys.* **30** (1963) 275.
- [7] G. Koster, L. Klein, W. Siemons, G. Rijnders, J. Dodge, C.-B. Eom, D. Blank, and M. Beasley, *Rev. Mod. Phys.* **84** (2012) 253.
- [8] L. Li, C. Richter, J. Mannhart, and R. Ashoori, *Nat. Phys.* **7** (2011) 762.
- [9] A. Honecker, J. Schulenburg, and J. Richter, *J. Phys.: Condens. Matter* **16** (2004) S749.
- [10] K. Siemensmeyer, E. Wulf, H.-J. Mikeska, K. Flachbart, S. Gabáni, S. Mařaš, P. Priputen, A. Efdokimova, and N. Shitsevalova, *Phys. Rev. Lett.* **101** (2008) 177201.
- [11] H. Kikuchi, Y. Fujii, M. Chiba, S. Mitsudo, T. Idehara, T. Tonegawa, K. Okamoto, T. Sakai, T. Kuwai, and H. Ohta, *Phys. Rev. Lett.* **94** (2005) 227201.
- [12] K. A. Gschneidner Jr. and V. K. Pecharsky, *Annu. Rev. Mater. Sci.* **30** (2000) 387.
- [13] K. A. Gschneidner Jr., V. K. Pecharsky, and A. O. Tsokol, *Rep. Prog. Phys.* **68** (2005) 1479.
- [14] K. A. Gschneidner Jr. and V. K. Pecharsky, *J. Rare Earths* **24** (2006) 641.
- [15] E. Bruck, O. Tegus, D. T. C. Thanh, and K. H. J. Buschow, *J. Magn. Magn. Mater.* **310** (2007) 2793.
- [16] K. Takada, H. Sakurai, E. Takayama-Muromachi, F. Izumi, R. A. Dilanian, and T. Sasaki, *Nature (London)* **422** (2003) 53.
- [17] Y. Kamihara, H. Hiramatsu, M. Hirano, R. Kawamura, H. Yanagi, T. Kamiya, and H. Hosono, *J. Am. Chem. Soc.* **128** (2006) 10012.
- [18] Y. Kamihara, T. Watanabe, M. Hirano, and H. Hosono, *J. Am. Chem. Soc.* **130** (2008) 3296.
- [19] T. Kimura, T. Goto, H. Shintani, K. Ishizaka, T. Arima, and Y. Tokura, *Nature* **426** (2003) 55.
- [20] N. Ikeda, H. Ohsumi, K. Ohwada, K. Ishii, T. Inami, K. Kakurai, Y. Murakami, K. Yoshii, S. Mori, Y. Horibe, and H. Kito, *Nature* **436** (2005) 1136.
- [21] S.-W. Cheong and M. Mostovoy, *Nature Mat.* **6** (2007) 13.
- [22] J. van den Brink and D. I. Khomskii, *J. Phys.: Condens. Matter* **20** (2008) 434217.
- [23] C. Lanczos, *J. Res. Nat. Bur. Stand.* **45** (1950) 255.
- [24] E. Dagotto, *Rev. Mod. Phys.* **66** (1994) 763.
- [25] A. L. Malvezzi, arXiv:cond-mat/0304375.
- [26] S. R. White, *Phys. Rev. Lett.* **69** (1992) 2863.
- [27] S. R. White, *Phys. Rev. B* **48** (1993) 10345.
- [28] M. E. J. Newman, G. T. Barkema, *Monte Carlo Methods in Statistical Physics*, Oxford, New York, 2001.
- [29] D. P. Landau and K. Binder, *A Guide to Monte Carlo Simulations in Statistical Physics*, Cambridge, 2015.
- [30] E. Engel and R. M. Dreizler, *Density Functional Theory*, Springer-Verlag Berlin, 2011.
- [31] M. S. S. Pereira, F. A. B. F. de Moura, and M. L. Lyra, *Phys. Rev. B* **77** (2008) 024402.
- [32] M. S. S. Pereira, F. A. B. F. de Moura, and M. L. Lyra, *Phys. Rev. B* **79** (2009) 054427.
- [33] M. E. Fisher, *Phys. Rev.* **113** (1959) 969.
- [34] I. Szyozi, In *Phase Transitions and Critical Phenomena*, edited by C. Domb and M. S. Green (Academic, New York, 1972), Vol. 1.
- [35] B. M. Lisnii, *Low Temp. Phys.* **37** (2011) 296.
- [36] B. M. Lisnyi, *Ukr. J. Phys.* **58** (2013) 195.
- [37] J. Čisárová and J. Strečka, *Acta Physica Polonica B* **45** (2014) 2093.
- [38] J. Čisárová and J. Strečka, *Phys. Lett. A* **378** (2014) 2801.
- [39] M. Nalbandyan, H. Lazaryan, O. Rojas, S. M. de Souza, and N. Ananikian, *J. Phys. Soc. Jpn.* **83** (2014) 074001.
- [40] L. Gálisová and J. Strečka, *Phys. Rev. E* **91** 022164 (2015).
- [41] L. Gálisová and J. Strečka, *Acta Physica Polonica A* **127** (2015) 216.
- [42] L. Gálisová and J. Strečka, *Phys. Lett. A* **379** (2015) 2474.
- [43] J. Strečka, A. Tanaka, L. Čanová, and T. Verkholyak, *Phys. Rev. B* **80** (2009) 174410.
- [44] L. Gálisová, J. Strečka, A. Tanaka, and T. Verkholyak, *Acta Physica Polonica A* **118** (2010) 942.
- [45] L. Gálisová, J. Strečka, A. Tanaka, and T. Verkholyak, *J. Phys.: Condens. Matter* **23** (2011) 175602.
- [46] F. F. Doria, M. S. S. Pereira, and M. L. Lyra, *J. Magn. Magn. Mater.* **368** (2014) 98.
- [47] M. Greiner, O. Mandel, T. Esslinger, T. W. Hansch, and I. Bloch, *Nature (London)* **415** (2002) 39.
- [48] S. Mukherjee, A. Spracklen, D. Choudhury, N. Goldman, P. Öhberg, E. Andersson, and R. R. Thomson, *Phys. Rev. Lett.* **114** (2015) 245504.
- [49] R. A. Vicencio, C. Cantillano, L. Morales-Inostroza, B. Real, C. Mejía-Cortés, S. Weimann, A. Szameit, and M. I. Molina, *Phys. Rev. Lett.* **114** (2015) 245503.
- [50] K. Noda, K. Inaba, and Makoto Yamashita, *Phys. Rev. A* **90** (2014) 043624.
- [51] D. Yoshioka, M. Mikuriya, and M. Handa, *Chem. Lett.* **31** (2002) 1044; M. Mikuriya, D. Yoshioka, and M. Handa, *Coord. Chem. Rev.* **250** (2006) 2194; T. E. Vos and J. S. Miller, *Angew. Chem. Int. Edn* **44** (2005)2416; J. S. Miller, T. E. Vos and W. W. Shum, *Adv. Mater.* **17** (2005) 2251.
- [52] O. Rojas, J. S. Valverde, and S. M. de Souza, *Physica A* **388** (2009) 1419.
- [53] J. H. Barry, M. Khatun, and T. Tanaka, *Phys. Rev. B* **37** (1988) 5193.
- [54] M. Khatun, J. H. Barry, and T. Tanaka, *Phys. Rev. B* **42** (1990) 4398.
- [55] J. H. Barry, T. Tanaka, M. Khatun, and C. H. Múnica, *Phys. Rev. B* **44** (1991) 2595.
- [56] J. H. Barry and M. Khatun, *Phys. Rev. B* **51** (1995) 5840.
- [57] S. Naya, *Prog. Theor. Phys.* **11** (1954) 53.
- [58] C. N. Yang, *Phys. Rev.* **85** (1952) 808.
- [59] R. B. Potts, *Phys. Rev.* **88** (1952) 352.
- [60] H. B. Callen, *Phys. Lett.* **4** (1963) 161.
- [61] M. Suzuki, *Phys. Lett.* **19** (1965) 267.
- [62] L. E. Reichl, *A Modern Course In Statistical Physics*, 2nd Edition, John Wiley & Sons, New Your, 1998.
- [63] J. Strečka, H. Čenčariková, and M. L. Lyra, *Phys. Lett. A* **379** (2015) 2915.
- [64] B. C. McEwan, *J. Chem. Soc.* **123** (1923) 2284.
- [65] T. Narayan and A. Kumar, *Phys. Rep.* **249** (1994) 135.
- [66] K. Binder and A. P. Young, *Rev. Mod. Phys.* **58** (1986) 801; H. Maletta and W. Zinn, *Handbook on the Physics and Chemistry of Rare Earths*, Vol. 12, edited by K. A. Gschneidner, Jr. and L. Eyring, Elsevier Science, Amsterdam, 1989, K. H. Fischer and J. Hertz, *Spin Glasses*, Cambridge University Press, Cambridge, 1991.
- [67] P. E. Cladis, *Phys. Rev. Lett.* **35** (1975) 48.
- [68] N. P. Kolmakova and A. A. Sidorenko, *J. Low Temp. Phys.* **28** (2002) 905.
- [69] G. Venturini, R. Welter, R. Ressouche, and B. Malaman, *J. Alloys. Compd.* **210** (1994) 213; R. Welter, G. Venturini, R. Ressouche, and B. Malaman, *J. Alloys. Compd.* **218** (1995) 204.
- [70] N. J. Ghimire, F. Ronning, D. J. Williams, B. L. Scott, Y. Luo, J. D. Thompson, and E. D. Bauer, *J. Phys.: Condens. Matter* **27** (2015) 025601.

phase	J'	Eigenvalue (E)	Eigenvector	border expression
0	$J' = 0$	$E(0) = -J'$	$ 0\rangle = \prod_{k=1}^{Nq/2} \pm 1\rangle_{\sigma_{k1}} \otimes 0, 0\rangle_k \otimes \pm 1\rangle_{\sigma_{k2}}$	$\mu < -\lambda$ (0-I)
	$J' < 0$		$ 0\rangle = \prod_{k=1}^{Nq/2} 1\rangle_{\sigma_{k1}} \otimes 0, 0\rangle_k \otimes -1\rangle_{\sigma_{k2}}$	$\mu < -\lambda - 2J'$ (0-I)
	$J' > 0$		$ 0\rangle = \prod_{k=1}^{Nq/2} 1\rangle_{\sigma_{k1}} \otimes 0, 0\rangle_k \otimes 1\rangle_{\sigma_{k2}}$	$\mu < -\omega$ (0-II)
I	$J' = 0$	$E(I) = -\lambda - \mu - J'$	$ \text{I}\rangle = \prod_{k=1}^{Nq/2} 1\rangle_{\sigma_{k1}} \otimes \frac{1}{\sqrt{2}} (\hat{c}_{k1,\uparrow}^\dagger + \hat{c}_{k2,\uparrow}^\dagger) 0, 0\rangle_k \otimes 1\rangle_{\sigma_{k2}}$	$-\lambda < \mu < \lambda - 2\omega$ (0-I-II)
	$J' < 0$			$-\lambda - 2J' < \mu < \lambda - 2\omega + 2J'$ (0-I-II)
	$J' > 0$			$-\lambda < \mu < \lambda - 2\omega + 2J'$ (0-I-II ₁)
II	$J' = 0$	$E(\text{II}/\text{II}_1) = -2\omega - 2\mu + J' $	$ \text{II}/\text{II}_1\rangle = \prod_{k=1}^{Nq/2} 1\rangle_{\sigma_{k1}} \otimes [a(\hat{c}_{k1,\uparrow}^\dagger \hat{c}_{k2,\downarrow}^\dagger) + b(\hat{c}_{k1,\downarrow}^\dagger \hat{c}_{k2,\uparrow}^\dagger) + c(\hat{c}_{k1,\uparrow}^\dagger \hat{c}_{k1,\downarrow}^\dagger) + d(\hat{c}_{k2,\uparrow}^\dagger \hat{c}_{k2,\downarrow}^\dagger)] 0, 0\rangle_k \otimes -1\rangle_{\sigma_{k2}}$	$\lambda - 2\omega + 2J' < \mu < -\lambda + 2\omega - 2J'$ (I-II/II ₁ -III)
	$J' < 0$			$-\omega < \mu < \omega$ (0-II-IV)
	$J' > 0$			$-\xi < \mu < \xi$ (I-II ₂ -III)
II	$J' = 0$	$E(\text{II}_2) = -2J - 2\mu - J'$	$ \text{II}_2\rangle = \prod_{k=1}^{Nq/2} 1\rangle_{\sigma_{k1}} \otimes (\hat{c}_{k1,\uparrow}^\dagger \hat{c}_{k2,\uparrow}^\dagger) 0, 0\rangle_k \otimes 1\rangle_{\sigma_{k2}}$	$-\xi < \mu < \xi$ (I-II ₂ -III)
	$J' < 0$	$E(\text{II}_3) = -2t - 2\mu - J'$		$\xi < \mu < -\xi$ (I-II ₃ -III)
	$J' > 0$	$E(\text{II}_3) = -2t - 2\mu - J'$		$\xi < \mu < -\xi$ (I-II ₃ -III)
III	$J' = 0$	$E(\text{III}) = -\lambda - 3\mu - J'$	$ \text{III}\rangle = \prod_{k=1}^{Nq/2} 1\rangle_{\sigma_{k1}} \otimes \frac{1}{\sqrt{2}} [\hat{c}_{k1,\uparrow}^\dagger \hat{c}_{k1,\downarrow}^\dagger \hat{c}_{k2,\uparrow}^\dagger - \hat{c}_{k1,\uparrow}^\dagger \hat{c}_{k2,\uparrow}^\dagger \hat{c}_{k2,\downarrow}^\dagger] 0, 0\rangle_k \otimes 1\rangle_{\sigma_{k2}}$	$-\lambda + 2\omega < \mu < \lambda$ (II-III-IV)
	$J' < 0$			$-\lambda + 2\omega - 2J' < \mu < \lambda + 2J'$ (II-III-IV)
	$J' > 0$			$-\lambda + 2\omega - 2J' < \mu < \lambda$ (II ₁ -III-IV)
IV	$J' = 0$	$E(\text{IV}) = -4\mu - J'$	$ \text{IV}\rangle = \prod_{k=1}^{Nq/2} \pm 1\rangle_{\sigma_{k1}} \otimes [\hat{c}_{k1,\uparrow}^\dagger \hat{c}_{k1,\downarrow}^\dagger \hat{c}_{k2,\uparrow}^\dagger \hat{c}_{k2,\downarrow}^\dagger] 0, 0\rangle_k \otimes \pm 1\rangle_{\sigma_{k2}}$	$\mu > \lambda$ (III-IV)
	$J' < 0$		$ \text{IV}\rangle = \prod_{k=1}^{Nq/2} 1\rangle_{\sigma_{k1}} \otimes [\hat{c}_{k1,\uparrow}^\dagger \hat{c}_{k1,\downarrow}^\dagger \hat{c}_{k2,\uparrow}^\dagger \hat{c}_{k2,\downarrow}^\dagger] 0, 0\rangle_k \otimes -1\rangle_{\sigma_{k2}}$	$\mu > \lambda + 2J'$ (III-IV)
	$J' > 0$		$ \text{IV}\rangle = \prod_{k=1}^{Nq/2} 1\rangle_{\sigma_{k1}} \otimes [\hat{c}_{k1,\uparrow}^\dagger \hat{c}_{k1,\downarrow}^\dagger \hat{c}_{k2,\uparrow}^\dagger \hat{c}_{k2,\downarrow}^\dagger] 0, 0\rangle_k \otimes 1\rangle_{\sigma_{k2}}$	$\mu > \omega$ (II-IV)
				$\mu > \lambda$ (III-IV)

Table 2: The list of eigenvalues, eigenvectors and border expressions for different phases from the ground-state phase diagrams corresponding to the investigated spin-electron model (1). Constants a , b , c and d used in the notation of eigenvectors II and II₁ have the following form: $a = \frac{1}{2} \left(\frac{J}{\sqrt{J^2 + t^2}} + 1 \right)$, $b = \frac{1}{2} \left(\frac{J}{\sqrt{J^2 + t^2}} - 1 \right)$ and $c = d = \frac{t}{2\sqrt{J^2 + t^2}}$. The notation λ , ω and ξ occurring in expressions for eigenvalues and border expressions are equal to $\lambda = J + t$, $\omega = \sqrt{J^2 + t^2}$ and $\xi = J - t$.